Article

Elucidating Potential Energy Surfaces for Singlet O_2 Reactions with Protonated, Deprotonated, and Di-Deprotonated Cystine Using a Combination of Approximately Spin-Projected Density Functional Theory and Guided-Ion-Beam Mass Spectrometry

Wenchao Lu,[†,‡] I-Hsien "Midas" Tsai,[§] Yan Sun,[†,‡] Wenjing Zhou,[†] and Jianbo Liu*,[†,‡]

[†]Department of Chemistry and Biochemistry, Queens College of the City University of New York, 65-30 Kissena Blvd., Queens, New York 11367, United States

[‡]Ph.D. Program in Chemistry, The Graduate Center of the City University of New York, 365 5th Avenue, New York, New York 10016, United States

[§]Department of Natural Sciences, LaGuardia Community College, 31-10 Thomson Avenue, Long Island City, New York 11101, United States

S *Supporting Information*

ABSTRACT: The reactivity of cystine toward electronically excited singlet O_2 ($a^1\Delta_g$) has been long debated, despite the fact that most organic disulfides are susceptible to oxidation by singlet O_2. We report a combined experimental and computational study on reactions of singlet O_2 with gas-phase cystine at different ionization and hydration states, aimed to determine reaction outcomes, mechanisms, and potential energy surfaces (PESs). Ion−molecule collisions of protonated and di-deprotonated cystine ions with singlet O_2, in both the absence and the presence of a water ligand, were measured over a center-of-mass collision energy (E_{col}) range from 0.1 to 1.0 eV, using a guided-ion-beam scattering tandem mass spectrometer. No oxidation was observed for these reactant ions except collision-induced dissociation at high energies. Guided by density functional theory (DFT)-calculated PESs, reaction coordinates were established to unravel the origin of the nonreactivity of cystine ions toward singlet O_2. To account for mixed open- and closed-shell characters, singlet O_2 and critical structures along reaction coordinates were evaluated using broken-symmetry, open-shell DFT with spin contamination errors removed by an approximate spin-projection method. It was found that collision of protonated cystine with singlet O_2 follows a repulsive potential surface and possesses no chemically significant interaction and that collision-induced dissociation of protonated cystine is dominated by loss of water and CO. Collision of di-deprotonated cystine with singlet O_2, on the other hand, forms a short-lived electrostatically bonded precursor complex at low E_{col}. The latter may evolve to a covalently bonded persulfoxide, but the conversion is blocked by an activation barrier lying 0.39 eV above reactants. At high E_{col}, C−S bond cleavage dominates the collision-induced dissociation of di-deprotonated cystine, leading to charge-separated fragmentation. Cross section for the ensuing fragment ion $H_2NCH(CO_2^-)CH_2SS^\bullet$ was measured as a function of E_{col}, and the mechanism of charge-separated fragmentation was discussed. It was also found that the reaction of deprotonated cystine with singlet O_2 follows a similar mechanism as that of di-deprotonated cystine, but with an even higher activation barrier (0.72 eV).
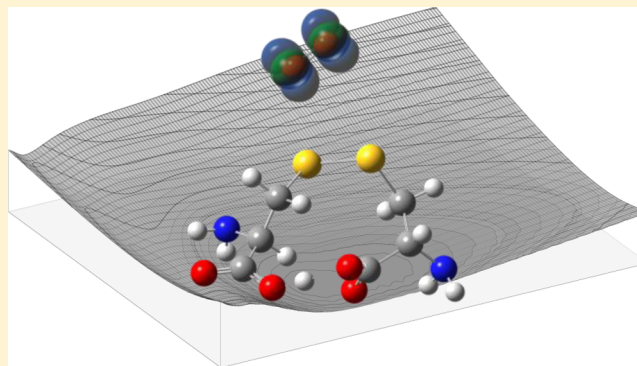
1. INTRODUCTION

The lowest electronically excited singlet $O_2[a^1\Delta_g]$ can be produced in biological systems by energy transfer to ground-state O_2 from protein-bound or other chromophores on exposure to UV−Vis light (i.e., photosensitized oxidation).[1] $^1O_2$ can also be generated by a range of endogenous enzymatic and chemical reactions.[2] Oxidation of biomolecules by $^1O_2$ leads to protein misfunctionality, mutagenic alterations to DNA, lipid peroxidation, and membrane degradation.[2−4] These oxidatively generated damages are involved in aging, mutation,

carcinogenesis, and cellular death, as well as in photodynamic therapy.[5]

Reactions of $^1O_2$ are highly selective and specific to certain residues in biological systems. Of the 20 "standard" amino acids that make up proteins, tryptophan (Trp), histidine (His), tyrosine (Tyr), methionine (Met), and cysteine (Cys) are the

five most susceptible to $^1O_2$ attack.[2] Oxidation of the thiol group of Cys may lead to the formation of a disulfide linkage with another Cys,[6] producing dimeric compound cystine (CySSCy). Disulfide bonds of cystine residues are responsible for the tertiary structures of polypeptides[7] and play a central role in stabilizing the correct, biologically active conformations of proteins against denaturation. Controlled oxidation of Cys and reduction of cystine act as a redox switch to control the structures and functions of a number of key proteins.[8] In addition to biological milieu, cystine is one of the amino acids abundant in tropospheric particles and depositions.[9,10] Questions have arisen as to whether cystine is vulnerable to further photodynamic oxidation in cells and to $^1O_2$-mediated photochemical transformations in the atmosphere.[11]

Studies on photobleaching of wool keratin implied possible reactions involving cystine with $^1O_2$.[12] However, many aspects of cystine oxidation (mechanism, products, kinetics, etc.) have not been well understood. It was suggested that cystine may react with $^1O_2$ in a manner similar to dialkyl sulfides and dialkyl disulfides,[13,14] that is, it forms a zwitterion persulfoxide $CySS^+(OO^-)Cy$, and the latter reacts with a second cystine to give rise to two molecules of $CySS(=O)Cy$.[15,16] However, the photosensitized oxidation experiments of cystine led to disputing results.[16,17] Murray and Jindal investigated methylene blue-sensitized photooxidation of cystine model compounds: 3,3-dithiobis(dipropionic acid), 3,3-dithiobis(dipropionic acid diethylamide), and cystamine.[18] Subsequently, Fliss and Viswanatha studied 2,3-butanedione-sensitized photooxidation of cystine.[19] All of these compounds were reported to be oxidized by $^1O_2$. In contradistinction to these observations, Weil reported that both cystine and S—S-glutathione were sluggish to photooxidation[20] (although in a previous report, Weil et al. reported that cystine was susceptible to methylene blue-sensitized photooxidation[21]). The nonreactivity of cystine toward $^1O_2$ was also observed by Iori et al. using other sensitizers.[22] It is not clear what might have been misinterpreted in the past studies. However, type I (radical-mediated) and type II ($^1O_2$-mediated) mechanisms may coexist in photooxidation and simultaneously contribute to reactions. Solution experimental results were also coupled to many other factors, for example, pH, solvent composition, type of sensitizer, and so forth. All of these apparently complicated the interpretation of photooxidation outcomes.

We have recently investigated the $^1O_2$ oxidation of protonated/deprotonated Cys[23−25] and Met[26,27] in the gas phase, in both the absence and the presence of water ligands. Experiments were carried out on a guided-ion-beam mass spectrometer, where reactions were separated from bulk solution environments. $^1O_2$ was produced through the reaction of H_2O_2 and Cl_2 in basic solution[28,29] without forming radical byproducts. Gas-phase experiments avoided the complexities arising from conventional solution-phase photooxidation experiments and eliminated the competition of $^1O_2$ oxidation with radical-mediated reactions. They have allowed us to distinguish intrinsic reactivities of amino acids toward $^1O_2$.

In the present work, we have extended gas-phase experiment to protonated/deprotonated cystine, aimed at directly measuring the reactivity of cystine with $^1O_2$. Experimental results were interpreted in light of density functional theory (DFT) calculations. To this end, B3LYP and BHandHLYP hybrid functionals were employed to characterize intermediates, products, and activation barriers. Owing to the mixing of open- and closed-shell characters of $^1O_2$ and reaction

intermediates,[30] closed-shell DFT methods led to large errors in energy calculations; on the other hand, broken-symmetry, open-shell DFT brought about spin contamination from high-spin states. To correct for spin contamination errors,[31] an approximate spin-projection method[32,33] was extended to the broken-symmetry, open-shell DFT calculations for cystine with $^1O_2$.

2. EXPERIMENTAL AND COMPUTATIONAL DETAILS

2.1. Gas-Phase $^1O_2$ Experiment. Reactions of cystine ions with $^1O_2$ were measured on a home-made guided-ion-beam tandem mass spectrometer.[34] The apparatus consists of an electrospray ionization (ESI) ion source, a radio frequency (rf) hexapole ion guide, a quadrupole mass filter, an rf octopole ion guide surrounded by a scattering cell, a second quadrupole mass filter, and a pulse-counting electron multiplier detector.

A sample solution for protonated $[CySSCy + H]^+$ was prepared by adding 48 mg of Cys (99%, Alfa Aesar) to 50 mL of 0.1 M HCl, leaving it overnight for complete dissolving, and then diluting to 0.004 mM with ethanol/water (3:1 vol. ratio). Solution for di-deprotonated $[CySSCy − 2H]^{2−}$ was prepared in ethanol/water (3:1) containing 0.2 mM cystine and 1.0 mM NaOH. According to cystine pK values (pK_1 1.50, pK_2 2.05, pK_3 8.03, and pK_4 8.80),[35] di-protonated $[CySSCy + 2H]^{2+}$ dominates at pH < 1.5, whereas deprotonated $[CySSCy − H]^-$ forms within a pH range of 7.5−9.3. Unfortunately, acidic solution of pH < 1.5 suppressed electrospray of cystine ions, whereas aqueous solution of pH 7−9 could not dissolve cystine. Therefore, neither $[CySSCy + 2H]^{2+}$ nor $[CySSCy − H]^-$ could be examined experimentally.

The solution of $[CySSCy + H]^+$ or $[CySSCy − 2H]^{2−}$ was sprayed into the ambient atmosphere through an electrospray needle at a rate of 0.06 mL/h. The ESI needle was held at 2.3 and −2.35 kV relative to ground for producing positively and negatively charged species, respectively. Charged droplets entered the source chamber of the mass spectrometer through the sampling aperture of a pressure-reducing desolvation capillary, which was heated to 140 °C and biased at 115 V for positive ions and −80 V for negative ones. The distance between the tip of the ESI needle and the sampling orifice of the capillary was 10 mm. Liquid aerosols underwent desolvation as they passed through the heated capillary and were converted to gas-phase ions in the source chamber. Under mild heating conditions, not all of the solvent was evaporated, resulting in the formation of both dehydrated and mono-hydrated ions. Ions were transported into the hexapole ion guide at a pressure of 24 mTorr, undergoing collisional focusing, and cooled to ∼310 K. Ions subsequently passed into a conventional quadrupole for selection of specific reactant ions. Reactant ions were collected into the octopole ion guide, which trapped ions in the radial direction. In addition to rf voltages, direct current (DC) bias voltage was applied to the octopole ion guide with variable amplitude to determine initial kinetic energy distributions of reactant ions using retarding potential analysis.[36] The DC bias voltage also allowed control of the kinetic energy of reactant ions in the laboratory frame (E_{Lab}), thereby setting the collision energy (E_{col}) between reactant ions and neutral gas molecules in the center-of-mass frame, that is, $E_{col} = E_{Lab} \times m_{neutral}/(m_{ion} + m_{neutral})$, where $m_{neutral}$ and m_{ion} are the masses of neutral and ionic reactants, respectively. The octopole passes through the scattering cell containing neutral reactant gas. The cell pressure was measured by a Baratron capacitance manometer (MKS 690 head and 670

signal conditioner). Product ions resulting from ion−molecule collisions and unreacted primary ions drifted to the end of the octopole and were mass-analyzed by the second quadrupole and counted by the electron multiplier. Intensities of the reactant ion beam were 5×10^4 counts/s for $[\text{CySSCy} + \text{H}]^+$, 1.4×10^5 counts/s for $[\text{CySSCy} - 2\text{H}]^{2-}$, and 2.4×10^4 counts/s for $[\text{CySSCy} - 2\text{H}]^{2-} \cdot \text{H}_2\text{O}$. Initial kinetic energy of the ion beam was 0.8 eV for $[\text{CySSCy} + \text{H}]^+$, 1.0 eV for $[\text{CySSCy} - 2\text{H}]^{2-}$, and 0.8 eV for $[\text{CySSCy} - 2\text{H}]^{2-} \cdot \text{H}_2\text{O}$, with an energy spread of 0.6 eV that corresponded to an E_{col} resolution better than 0.1 eV.

$^1\text{O}_2$ was generated by the reaction of $\text{H}_2\text{O}_2 + \text{Cl}_2 + 2\text{KOH} \rightarrow {}^1\text{O}_2/{}^3\text{O}_2 + 2\text{KCl} + 2\text{H}_2\text{O}$.[26,37] KOH (10.5 mL, 8 M) was added to 20 mL of 35 wt % aqueous H_2O_2 in a sparger held at −16 °C. The resulting mixture was degassed. Cl_2 (4.4 sccm, ~99.5%, Sigma-Aldrich) was mixed with 96 sccm of He and bubbled through the H_2O_2/KOH slush. All of the Cl_2 reacted with H_2O_2 to produce a mixture of $^1\text{O}_2$, $^3\text{O}_2$, and water.[26,37] Gas products passed through a −70 °C cold trap to remove water vapor. Only $^1\text{O}_2$, $^3\text{O}_2$, and He remained in the gas mixture. Before leaking into the scattering cell of the mass spectrometer for ion−molecule collisions, the concentration of $^1\text{O}_2$ was determined by measuring $^1\text{O}_2$ emission $(\text{a}^1\Delta_g \rightarrow \text{X}^3\textstyle\sum_g^-)$[38] at 1270 nm in an optical emission cell.[26] The scattering cell pressure was set at 0.25 mTorr containing 5% of $^1\text{O}_2/{}^3\text{O}_2$ and 95% of He. Under these conditions, cystine ions underwent at most a single collision with O_2. Ions also collided with He, but heavy ion−light neutral combination made these collisions insignificant at experimental E_{col}. The $^1\text{O}_2$ generator also produced $^3\text{O}_2$. To determine if reactions are $^1\text{O}_2$ specific, control experiments were performed under the same conditions using pure $^3\text{O}_2$.

2.2. Electronic Structure Calculations and the Approximate Spin-Projection Method. Structures of reactants, intermediates, transition states (TSs), and products were optimized at the B3LYP level of theory paired with 6-31+G(d,p) and 6-311++G(d,p) basis sets using Gaussian 09.[39] Tautomer/rotamer search was conducted for cystine ions, and the most stable conformations were used as starting structures in construction of reaction potential energy surfaces (PESs). B3LYP-calculated vibrational frequencies and zero-point energies were scaled by a factor of 0.952 and 0.981,[40] respectively. All TSs were verified as first-order saddle points, and the vibrational mode associated with an imaginary frequency corresponds to the anticipated reaction pathway. Aside from the local criterion, intrinsic reaction coordinate (IRC) calculations were carried out to identify reactant and product minima connected through the identified TSs. PES scans were carried out using B3LYP and RI-MP2 with the same basis set 6-31+G(d,p). RI-MP2 calculations were completed using ORCA 4.0.0.2.[41] Charge populations were analyzed using NBO 6.0.[42] RRKM[43] unimolecular rates were calculated with the program of Zhu and Hase,[44] using direct state count algorithm.

For the reasons discussed above, closed-shell DFT and MP2 methods led to large errors in the calculations of $^1\text{O}_2$ excitation energy, and MP2 overestimated the diatomic bond length by ~0.1 Å. On the other hand, broken-symmetry, open-shell calculations ran into spin contamination from $^3\text{O}_2$ that adversely affects the quality of calculations, too. In our previous studies,[23,25] the DFT energy of $^1\text{O}_2$ was obtained by adding the experimental excitation energy of 0.98 eV[38] to the DFT energy of $^3\text{O}_2$. But the spin contamination problem exists not only for reactant but also in the reaction intermediate region,[45] where the contamination from triplet states shifts the energies of stationary points and TSs. Therefore, for intermediates that were invalidated by large contributions from species other than Hartree−Fock configurations, we had utilized the multi-reference CASMP2//CASSCF method.[46,47] However, application of CASSCF to the present system of 16 heavy atoms is impractical in terms of computational cost. Yamaguchi and co-workers developed an approximate spin-projection method to remove spin contamination errors from broken-symmetry singlet states.[32,33] The approach was assessed at various DFT levels (including B3LYP and BHandHLYP) using the cyclo-addition of $^1\text{O}_2$ to ethylene as a test, which goes through a diradical intermediate. More recently, Schlegel and co-workers have applied the same method to the $^1\text{O}_2$ oxidation of guanine[48] and obtained satisfactory results. Inspired by these works, we have adopted spin-projected broken-symmetry, open-shell DFT calculations in the present study.

3. RESULTS AND DISCUSSION

3.1. Structures of Protonated, Deprotonated, and Di-Deprotonated Cystine. Cystine ions have numerous conformations. To find the global minima of their conformational landscape, a grid search method was applied. We rotated each of the torsion angles along molecules through 360° at 60° increments to generate trial staggered conformations for each ionization state. Every conformation so generated was subjected to optimization at B3LYP/6-31+G(d) to derive the associated local minimum conformation. Many of the initial conformations optimized to the same local minima. All local minimum conformations were reoptimized at B3LYP/6-311++G(d,p). For each ionization state, all of the conformers with relative energy within 0.2 eV are provided in the Supporting Information together with their Cartesian coordinates and energies. Each conformer has a number suffix to indicate the order of stability within its category. We have compared relative energies of conformers at a pressure of 1 atm versus mTorr and found no obvious changes. Major conformers for each series are summarized in Figure 1.

For $[\text{CySSCy} + \text{H}]^+$, a total of 14 stable conformers/rotamers were located within 0.2 eV. They are gathered in Figure S1, of which the two most significant, $[\text{CySSCy} + \text{H}]^+\_1$ and 2, are depicted in the top row of Figure 1. These two conformers represent 54 and 34% of protonated ions at 298 K, respectively. In both conformers, two amino groups interact to stabilize the proton. Seven low-energy conformers were identified for $[\text{CySSCy} - \text{H}]^-$ (Figure S2). The first three lowest-energy conformers lie within 0.1 eV with a population of 69, 15, and 14%, respectively. Both protonated and deprotonated cystines are featured by cyclic structures via proton sharing and charge complexation between two Cys residues. A total of 23 $[\text{CySSCy} - 2\text{H}]^{2-}$ conformers lie within 0.2 eV, as summarized in Figure S3. In contrast to cyclization of singly charged structures, $[\text{CySSCy} - 2\text{H}]^{2-}$ is constrained to linear structures, to maximize the distance and thus minimize Coulomb repulsion between the two negative charges. The two lowest-energy conformers, accounting for 44 and 33% of the population, have the two carboxylate termini separated from each other more than 9 Å.

Our conformation search not only reproduced the protonated cystine conformers that were reported at the B3LYP/6-31+G(d,p) and RI-MP2 levels of theory,[49] but also found many new structures and identified new global minima.
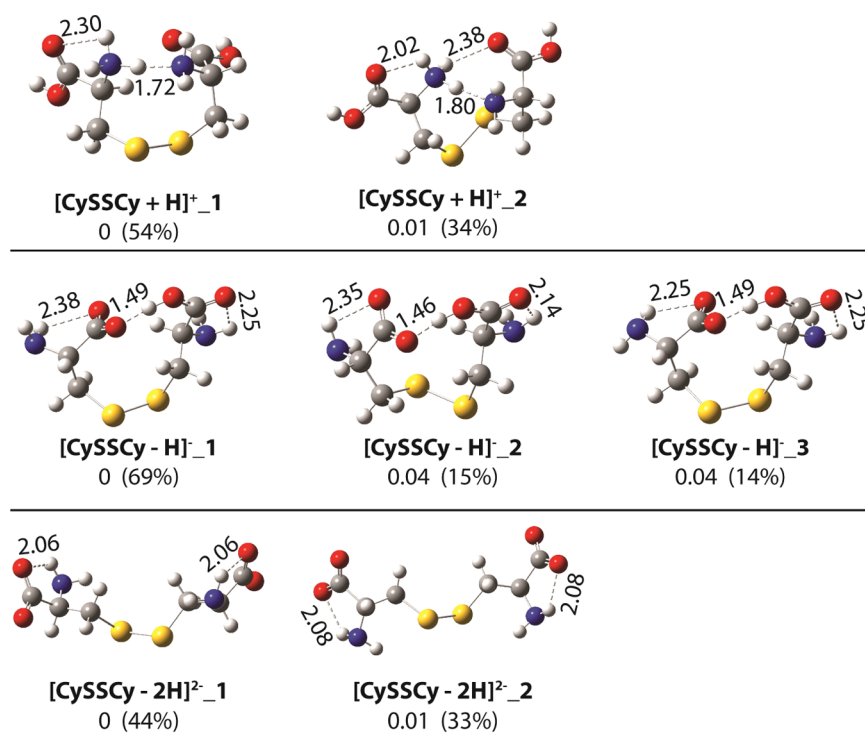
Figure 1. Low-lying tautomers/conformers of $[CySSCy + H]^+$, $[CySSCy − H]^−$, and $[CySSCy − 2H]^{2−}$. Relative energies (eV, with respect to global minima) and thermal populations (in parentheses) were evaluated at B3LYP/6-311++G(d,p) with 298 K thermal corrections.

On the basis of calculated populations, $[CySSCy + H]^+\_1$, $[CySSCy − H]^−\_1$, and $[CySSCy − 2H]^{2−}\_1$ in Figure 1 represent dominating reactant ions in gas-phase experiments and were used as starting structures in PESs. It is certainly possible that interconversion between different conformers may occur during ion–molecule collisions. However, it seems less likely that different conformers would significantly alter reaction coordinates, as confirmed by direct dynamics trajectory simulations of protonated/deprotonated Cys with $^1O_2$.[23−25]

3.2. Products from Ion–Molecule Collisions. *3.2.1. [CySSCy + H]$^+$ + $^1O_2$.* We started by first examining the reaction of $[CySSCy + H]^+$ (m/z 241) over the center-of-mass E_{col} range of 0.1−1.0 eV. Product ions were observed at m/z 120, 152, 154, 195, and 223. A representative product ion mass spectrum and formation scheme are illustrated in Figure S4 in the Supporting Information. Product ions of m/z 120 are due to bond cleavage at the disulfide link.[50−52] Its structure could be assigned to $H_2NCH(CO_2H)CH_2S^+$ (i.e., $[Cys − H]^+$, see Figure S4),[51] and the S−S bond rupture was preceded by an intramolecular proton transfer from the ammonium group to the disulfide bond. Although m/z 120 is minor in collision-induced dissociation (CID), the same fragment is dominant in electron-induced dissociation (EID) of $[CySSCy + H]^+$.[52] The m/z 152 can be attributed to cyclic $[−^+H_2NCH(CO_2H)-CH_2SS−]$,[50−54] produced by C−S cleavage via a Grob-like fragmentation process.[51] The m/z 154 might be assigned as a protonated thiocysteine $H_3N^+CH(CO_2H)CH_2SSH$.[51−53] Product ions of m/z 195 and 223 correspond to concomitant loss of neutral (H_2O + CO) and elimination of a single water from $[CySSCy + H]^+$, respectively.[51−53]

All of these products were observed also upon collisions of $[CySSCy + H]^+$ with ground-state O_2 and therefore could be excluded from $^1O_2$-specific reactions. Intensities of most product ions increased at high E_{col}, except for m/z 120 that

had only a small amount and diminished at high energies. The latter does not resemble typical CID, in which high collision energy would enhance fragmentation.

3.2.2. [CySSCy − 2H]$^{2−}$ + $^1O_2$ and Disulfide Bond Cleavage. For $[CySSCy − 2H]^{2−}$ (m/z 119) + $^1O_2$, only four CID product ions were detected, as shown in Figure 2a along with fragmentation scheme. The first three correspond to m/z 73 ($H_2N\dot{C}HCO_2^−$), 110 (elimination of a water from $[CySSCy − 2H]^{2−}$), and 101 (elimination of two water molecules from reactant ion), all of which have minor intensities. The major product is an anionic radical $H_2NCH-(CO_2^−)CH_2SS^•$ at m/z 151. m/z 151 could also be assigned to $H_2NCH(CO_2^−)CH_2SO_2$—a product that may form by breaking the S−S bond of an O_2 adduct $[CySS(OO)Cy − 2H]^{2−}$. To identify the structure of m/z 151, an isotopic labeling experiment was carried out using $[Cy^{32}S^{34}SCy − 2H]^{2−}$ (m/z 120) as the reactant ion. If $H_2NCH(CO_2^−)CH_2SO_2$ were produced, the product would have contained a mixture of m/z 151 (containing a ^{32}S) and 153 (containing a ^{34}S) with a 1:1 intensity ratio. However, only a single ion peak was observed at m/z 153, consistent with the structure of $H_2NCH(CO_2^−)-CH_2^{32}S^{34}S^•$.

The observation that CID of $[CySSCy − 2H]^{2−}$ is dominated by C−S cleavage is consistent with the previous report that the absence of a mobile proton facilitates disulfide bond cleavage.[51] Identical product ions were obtained in the collisions of $[CySSCy − 2H]^{2−}$ with pure $^3O_2$ and Ar. We have measured the cross sections of the product ion $H_2NCH-(CO_2^−)CH_2SS^•$ in collisions of $[CySSCy − 2H]^{2−}$ with O_2 and Ar. Cross sections were determined from the ratios of reactant to product ion intensities at each E_{col}, the pressure of collision gas in the scattering cell, and the effective cell length. Results are plotted in Figure 2b over the E_{col} range from 0.1 to 5 eV. The two collision systems present similar "apparent" thresholds
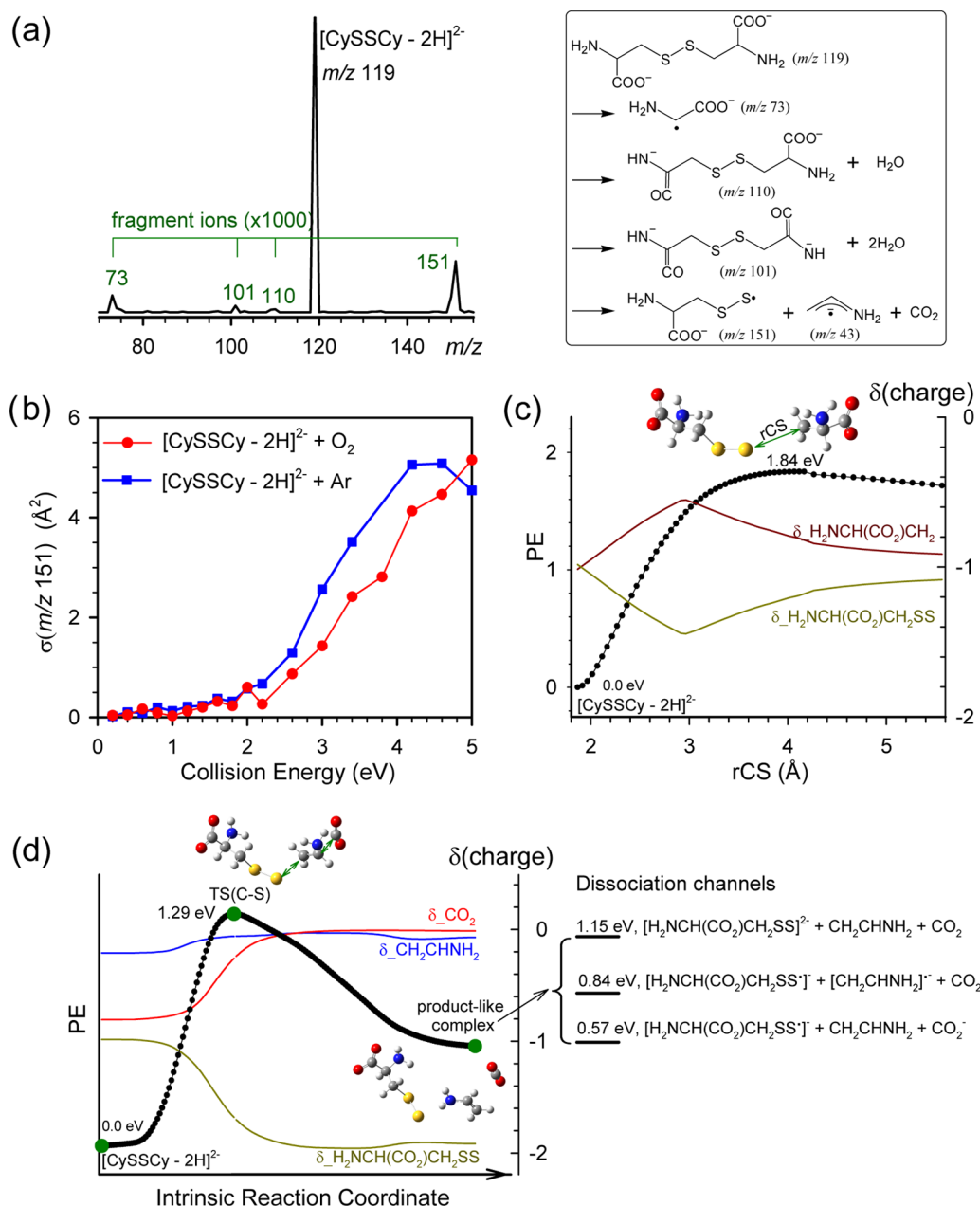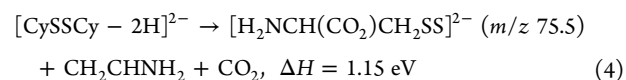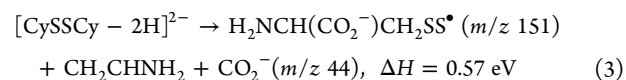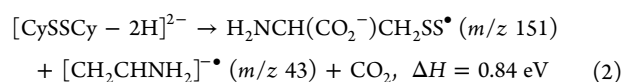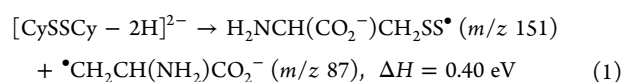
Figure 2. (a) Product mass spectrum for $[CySSCy - 2H]^{2-} + {}^1O_2$ obtained at $E_{col} = 1.0$ eV, and fragmentation scheme. (b) Cross sections for product ion m/z 151 in collisions of $[CySSCy - 2H]^{2-}$ with oxygen and Ar. (c) Open-shell C−S bond dissociation PES for $[CySSCy - 2H]^{2-}$ and product charge distributions, calculated at uB3LYP/6-31+G(d,p). (d) Closed-shell IRC trajectory for C−S bond cleavage of $[CySSCy - 2H]^{2-}$, and changes of product charge partitions, calculated at B3LYP/6-311++G(d,p). Vibrational mode corresponding to TS(C−S) imaginary frequency is indicated by displacement vectors. A movie of TS(C−S) along reaction pathway is available in the Supporting Information.

for production of $H_2NCH(CO_2^-)CH_2SS^\bullet$. At high E_{col}, Ar produced slightly larger cross sections.

On the basis of PES scans and stationary-point calculations at B3LYP/6-311++G(d,p), the C−S cleavage of $[CySSCy - 2H]^{2-}$ may occur via four possible pathways

$$[CySSCy - 2H]^{2-} \rightarrow H_2NCH(CO_2^-)CH_2SS^\bullet \ (m/z \ 151)$$
$$+ {}^\bullet CH_2CH(NH_2)CO_2^- \ (m/z \ 87), \ \Delta H = 0.40 \ \text{eV} \quad (1)$$

$$[CySSCy - 2H]^{2-} \rightarrow H_2NCH(CO_2^-)CH_2SS^\bullet \ (m/z \ 151)$$
$$+ [CH_2CHNH_2]^{-\bullet} \ (m/z \ 43) + CO_2, \ \Delta H = 0.84 \ \text{eV} \quad (2)$$

$$[CySSCy - 2H]^{2-} \rightarrow H_2NCH(CO_2^-)CH_2SS^\bullet \ (m/z \ 151)$$
$$+ CH_2CHNH_2 + CO_2^- (m/z \ 44), \ \Delta H = 0.57 \ \text{eV} \quad (3)$$

$$[CySSCy - 2H]^{2-} \rightarrow [H_2NCH(CO_2)CH_2SS]^{2-} \ (m/z \ 75.5)$$
$$+ CH_2CHNH_2 + CO_2, \ \Delta H = 1.15 \ \text{eV} \quad (4)$$

Reaction 1 produces two radical anions. Despite being the least endothermic, this reaction bears the highest activation barrier (1.84 eV) and thus is energetically less favorable than reactions 2−4 that are to be discussed blow. The height of the reaction 1 barrier is partly attributed to the intramolecular repulsive Coulomb barrier (RCB) against charge-separated fragmentation. Here, the RCB is created as a result of the superposition of

short-range binding of excess charges in the dianion and long-range Coulomb repulsion between two negatively charged fragments.[55,56] The open-shell dissociation PES for reaction 1 is shown in Figure 2c, obtained by relaxed PES scan along the dissociating $rC-S$ bond using uB3LYP/6-31+G(d,p).

Reactions 2−4 are governed by a single transition state TS(C−S) of 1.29 eV, as shown in Figure 2d. TS(C−S) is located at the early stage of the reactions, and its imaginary frequency corresponds to the motions of dissociating both C−S and CH−COO$^-$ bonds simultaneously, as indicated by green displacement vectors. A movie of TS(C−S) along the reaction path is available in the Supporting Information. The structures of the reactant and product minima connected through TS(C−S) were verified by IRC trajectory calculation. Once crossing TS(C−S), the system forms a product-like complex. The latter may produce three sets of fragments via reactions 2−4 that differ only in which fragments carry charges. Their energetics are indicated by bold lines in the figure. Reaction 4 could be ruled out because no dianionic product $[H_2NCH(CO_2)CH_2SS]^{2-}$ was detected in the experiment. The absence of this reaction is not surprising because this dissociation channel has the largest endothermicity among reactions 2−4, so the system switches to low-energy electronic state(s) that may lead to reactions 2 and/or 3. The likelihood for reactions 2 and 3 depends on the extent of charge delocalization and the nature of how charge states start to "unmix" as products separate. In theory, product branching between (2) and (3) could be determined by the intensities of the complementary ions $[CH_2CHNH_2]^{-\bullet}$ and CO_2^- that were produced concurrently with $H_2NCH(CO_2^-)CH_2SS^\bullet$ in reactions 2 and 3. Unfortunately, neither of the two complementary ions was present in product ion mass spectra—a not unusual phenomenon in CID of multiply charged ions.[57,58]

Natural population analysis indicates that the charges of the $H_2NCH(CO_2)CH_2SS$, CH_2CHNH_2, and CO_2 moieties are −1.68, −0.06, and −0.26 at TS(C−S), respectively, and the CO_2 moiety has a $\angle O-C-O$ bend angle of 154°, which is closer to CO_2^- anion (138°) than to neutral CO_2 (180°). The question is at what point and how the charge separation among fragments gets decided. Figure 2d tracks the charges upon individual moieties along the IRC trajectory. The CO_2 moiety starts to lose negative charge as soon as the trajectory approaches the activation barrier and becomes neutral after the trajectory crosses over TS(C−S). Charges between $H_2NCH(CO_2)CH_2SS$ and CH_2CHNH_2, on the other hand, mix together during the trajectory. Both open- and closed-shell DFT calculations converged to the same product-like complex. Within this complex, charge populations are −1.9 on $H_2NCH(CO_2)CH_2SS$, −0.1 on H_2NCHCH_2, and none on CO_2. It seems that RCB is sufficiently large to bind excess electrons within a single $H_2NCH(CO_2)CH_2SS$ moiety. We speculate that charge separation between $H_2NCH(CO_2)CH_2SS$ and CH_2CHNH_2 did not occur until the final stage when products start to separate beyond equilibrium distance.

A similar late-stage charge separation scenario was reported for $H_2CO^+ + C_2H_4 \rightarrow HCO^+ + C_2H_5$ and $HCO + C_2H_5^+$.[59] In this reaction, two product channels (a pair of charge states for $[HCO + C_2H_5]^+$) share a common transition state, which leads to the formation of a product-like complex. Actual atom transfer takes place in the geometry where reactants are interacting intimately, and charge separation occurs at the last step when products separate. Such late-stage charge separation was verified by the competition between the two product

channels and their dependence on E_{col} and H_2CO^+ vibrational modes.

The branching between reactions 2 and 3 must depend on how the energies and coupling strength of these charge states vary with separation. It would be ideal to follow charge separation and dissociation of the product-like complex in Figure 2d and locate the barrier on the PES that leads to two separate valleys. We note that the reaction of $[CySSCy - 2H]^{2-}$ takes place on a single potential surface up to the product-like complex and then undergoes a transition from one electronic state to another. This electronic−state transition is evidenced by the formation of charge-separated products rather than dianionic $[H_2NCH(CO_2)CH_2SS]^{2-}$. However, the DFT method used for PES calculations is not applicable to this nonadiabatic intersystem crossing or surface hopping, particularly when the transition between the two charge states is abrupt. In addition, near the crossing seam, a single reference wavefunction may be inadequate for calculations. For these reasons, we did not attempt to calculate the branching between reactions 2 and 3.

We have also calculated the symmetric S−S bond-rupture process of $[CySSCy - 2H]^{2-} \rightarrow 2[Cys - H]^{-\bullet}$ (anionic radical, m/z 119). The reaction has ΔH of only 0.2 eV calculated at B3LYP/6-311++G(d,p) but bears a dissociation barrier of 2.5 eV and thus is not expected to be accessible during low-energy CID. We could not rule out the possibility of S−S cleavage at high E_{col}. However, product ion $[Cys - H]^{-\bullet}$ has the same m/z as the reactant and thus could not be distinguished by mass spectrometry.

The adiabatic electron detachment energy for $[CySSCy - 2H]^{2-}$ was calculated to be 1.2 eV at B3LYP/6-31+G(d,p). The unfavorable electron detachment is related to the fact that the resulting anionic radical tends to eliminate two CO_2 moieties. Charge transfer between $[CySSCy - 2H]^{2-}$ and $^1O_2$ is, on the other hand, exothermic by 0.26 eV. Nevertheless, neither electron detachment nor charge transfer was observed in the experiment. The inability to detect these reactions may be again due to the existence of RCB. It follows that energy substantially higher than the electron-binding energy is required to remove an electron from $[CySSCy - 2H]^{2-}$.

We note that none of the aforementioned reactions are $^1O_2$ specific. We had thought that the failure to detect oxidation products of cystine ions might be because the peroxides formed in the reactions were unstable and did not have sufficient lifetime, and in the meantime, their conversions to end products were blocked by high-energy barriers. Consequently, intermediates could only decay back to reactants via physical quenching of $^1O_2$. Such scenario indeed happened in the $^1O_2$ reactions with gas-phase Cys[23−25] and Met,[27] where the decay of transient hydroperoxides CySOOH and MetOOH caused fragmentation of amino acids. For those systems, we devised reaction routes using hydrated Cys and Met as the targets for collisions with $^1O_2$. The point was to stabilize hydroperoxides via water-evaporation cooling of gas-phase hydrates. This strategy was proved to be successful in capturing CySOOH and MetOOH. Following the same idea, we examined the collisions of $^1O_2$ with monohydrated $[CySSCy - 2H]^{2-}\cdot H_2O$. Contrary to our expectation, no oxidation product was detected for hydrated reactant ions, either.

3.3. Reaction PESs. *3.3.1. Repulsive PES for [CySSCy + H]$^+$ + $^1O_2$.* To address the origin of the nonreactivity of $[CySSCy + H]^+$ with $^1O_2$, a 31 × 19 grid reaction PES was generated at B3LYP/6-31+G(d,p). The contour map is visualized in Figure

3a along rSO (the distance between the reacting S and O atoms) and rSS (the disulfide bond length). During the PES
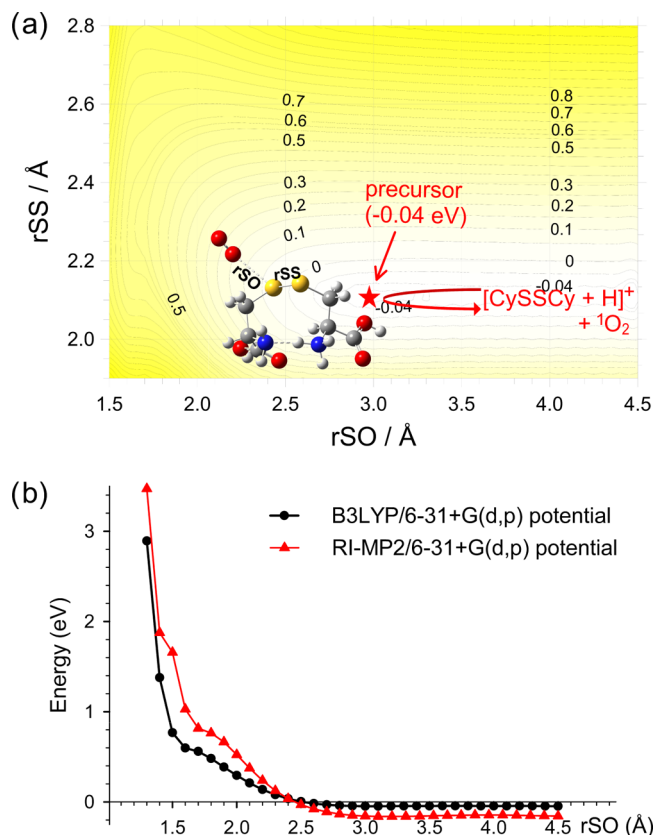

Figure 3. (a) Two-dimensional PES for $[CySSCy + H]^+ + {}^1O_2$. Numbers in contour map are potential energies calculated at B3LYP/6-31+G(d,p). (b) B3LYP- vs RI-MP2-calculated PESs for $[CySSCy + H]^+ + {}^1O_2$.

scan, rSO and rSS varied from 4.5 to 1.5 Å and 1.9 to 2.8 Å at intervals of 0.1 and 0.05 Å, respectively. All of the other bond lengths and bond angles were optimized at each point of the PES. On this PES, there is a strip of flat and shallow potential well leading from the reactants to a precursor complex located at rSO = 3.0 Å and rSS = 2.1 Å with a binding energy of only 0.04 eV. The amount of binding energy roughly matches the charge-induced dipole potential at an ion−molecule center-of-mass distance of 4 Å.[60] The fact that the potential becomes repulsive at rSO < 2.5 Å implies that either ${}^1O_2$ is well shielded from the positive charge of the protonated amino group or the ion-induced dipole term is weaker than the repulsion between reactants.

We noticed that DFT was reported to be problematic in describing dimethyl persulfoxide $((CH_3)_2SOO)$.[45] The stable B3LYP structure for $(CH_3)_2SOO$ was characterized by a long rSO distance of 2.36 Å. On the other hand, MP2 was able to locate a covalently bound $(CH_3)_2SOO$ with rSO of 1.59−1.65 Å.[45,61] In our PES study for $[CySSCy − H]^- + {}^1O_2$ and $[CySSCy − 2H]^{2-} + {}^1O_2$ (vide infra), DFT was able to locate both weakly bound precursor complexes (rSO = 2.4 Å) and covalently bonded cystine persulfoxides (rSO = 1.7 Å), as well as the transition states connecting the two structures. To further ascertain that the short-range potential surface was not artificially raised by DFT, another PES scan was completed along rSO at the RI-MP2 level of theory. The RI-MP2 method

is almost equivalent to the exact MP2 in calculating ${}^1O_2$ reaction PESs[62] but with a higher computational efficiency. The similarities and differences between DFT and RI-MP2 PESs are illustrated by comparing the two relaxed PESs in Figure 3b, which were calculated at the same collision orientations and using the same basis set. As shown in the figure, the RI-MP2 curve has a slightly deeper well at large reactant separation. Both curves become repulsive starting at rSO = 2.5 Å, and the RI-MP2 potential increases more quickly at short range.

During ion−molecule collisions, as the distance between reactants decreases, the kinetic energy, which was initially wholly translational, was being converted to centrifugal energy.[63] We have estimated the orbital angular momentum (L) for the collision complex at $E_{col} = 0.1$ eV, using $L = \mu \cdot v_{rel} \cdot (\sigma_{collision}/\pi)^{1/2}$, where μ and v_{rel} are the reduced mass and relative velocity of the collision partners, respectively, and $\sigma_{collision}$ is the ion-induced dipole-capture cross section.[60] Resulting centrifugal barrier for the calculated L reaches ∼0.1 eV at rSO of 3−4 Å. Therefore, total potential, as the sum of ion−molecule potential and centrifugal barrier, becomes consistently repulsive as ${}^1O_2$ approaches $[CySSCy + H]^+$.

3.3.2. $[CySSCy − H]^-$ and $[CySSCy − 2H]^{2-}$ May Form Persulfoxides with ${}^1O_2$. We have mapped out reaction PESs for both $[CySSCy − H]^-$ and $[CySSCy − 2H]^{2-}$ at B3LYP/6-31+G(d,p) in Figure 4 so that we may look at the effects of an excess negative charge on the reaction. To differentiate similar structures between singly and di-deprotonated ones, we included the number of missing protons and negative charge in their acronyms. The two PESs share common features and so they are described together. Both $[CySSCy − H]^-$ and $[CySSCy − 2H]^{2-}$ may form precursor complexes with ${}^1O_2$ at the early stage of collisions, and their binding energies are −0.37 and −0.46 eV, respectively. Critical bond lengths are rSO = 2.49 and 2.38 Å, rOO = 1.26 and 1.27 Å, and rSS = 2.08 and 2.10 Å for the singly and di-deprotonated precursors, respectively. In contrast to the protonated precursor that bounces off the repulsive potential surface, both singly and di-deprotonated precursors may evolve to high-energy but stable covalently bound persulfoxides. A minimum-energy pathway along intrinsic reaction coordinate is projected onto each of the two PESs. IRC trajectories feature the so-called "late-barriers" located at $[TS − H]^-$ and $[TS − 2H]^{2-}$ (the movies of $[TS − H]^-$ and $[TS − 2H]^{2-}$ along reaction pathways are available in the Supporting Information). The transition states resemble their products in geometries except the changes of three bond lengths, that is, rSO = 1.76 versus 1.64 Å, rSS = 2.17 versus 2.21 Å, and rOO = 1.37 versus 1.43 Å for $[TS − H]^-$ and $[CySS(OO)Cy − H]^-$; and rSO = 1.85 versus 1.68 Å, rSS = 2.14 versus 2.15 Å, and rOO = 1.35 versus 1.40 Å for $[TS − 2H]^{2-}$ and $[CySS(OO)Cy − 2H]^{2-}$, respectively.

The only difference between the PESs for $[CySSCy − H]^-$ and $[CySSCy − 2H]^{2-}$ concerns the long-range potential. $[CySSCy − 2H]^{2-}$ remains attractive to ${}^1O_2$ at large separations and has a binding energy of 0.2 eV with ${}^1O_2$ at rSO = 4.5 Å, whereas the attractive potential between $[CySSCy − H]^-$ and ${}^1O_2$ decreases quickly at large SO. This difference might be attributed to two facts. First, long-range ion-induced dipole potential ($= -\alpha q^2/2r^4$, where α is the molecule polarizability, q is the ion charge, and r is the ion−molecule separation) increases with ion charges. Second, at relatively large reactant separation, ${}^1O_2$ could be locked into orientations close to the $−NH_2$ and/or $−CO_2^-$ groups of $[CySSCy − 2H]^{2-}$. Electro-
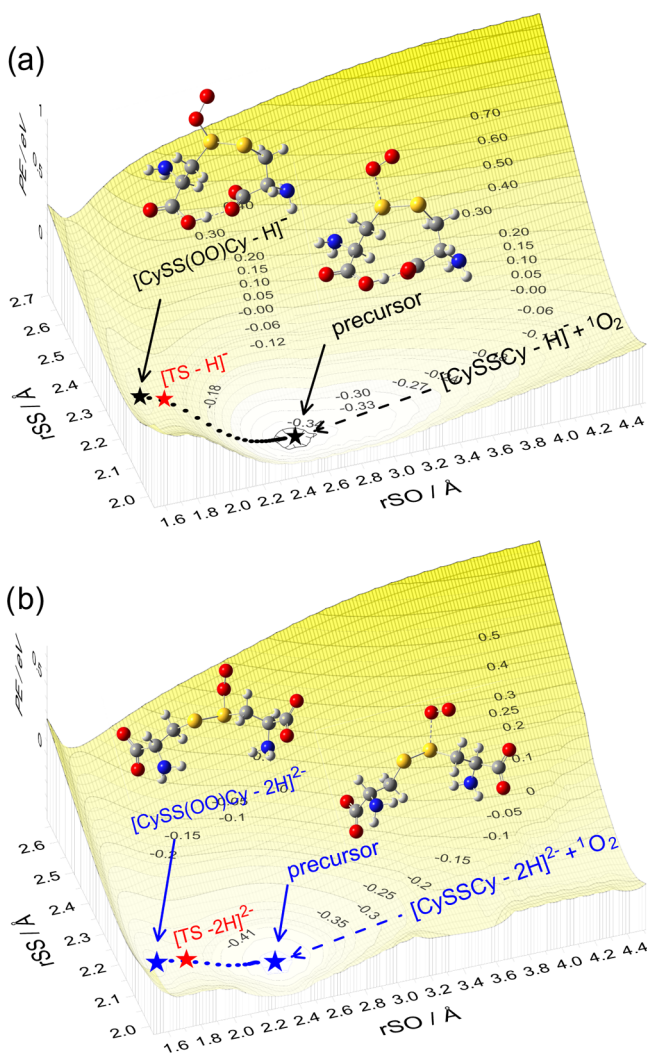
Figure 4. Two-dimensional PESs for (a) $[CySSCy - H]^- + {}^1O_2$ and (b) $[CySSCy - 2H]^{2-} + {}^1O_2$. Numbers in the contour maps are potential energies calculated at B3LYP/6-31+G(d,p). Dotted lines represent IRC trajectories. Movies of $[TS - H]^-$ and $[TS - 2H]^{2-}$ along reaction pathways are available in the Supporting Information.

static binding energy at such orientations reaches up to 0.7 eV. Formation of these electrostatic complexes becomes most probable when ${}^1O_2$ attacks the back side of the disulfide bond and the two termini of $[CySSCy - 2H]^{2-}$. Nevertheless, trapping in these collision complexes disfavors the attack of ${}^1O_2$ on the disulfide bond.

3.3.3. Reaction Coordinates Refined by an Approximate Spin-Projection Method. Guided by the PESs in Figures 3 and 4, we are able to establish reaction coordinates for all three systems. ${}^1O_2$ reactions present multiconfigurational characters and thus lead to poorly calculated stationary-point energies and barrier heights using restricted DFT. Calculating energies for the present systems using multireference solutions, such as CASMP2,[47] was not feasible due to large system sizes. Here, approximately spin-projected open-shell, broken-symmetry B3LYP calculations were used to refine local minima and TSs. The spin contamination error was approximately removed following Yamaguchi's methodology described by eq 5

$$E^{AP} = E^{BS} \frac{\langle S^2 \rangle^{HS}}{\langle S^2 \rangle^{HS} - \langle S^2 \rangle^{BS}} - E^{HS} \frac{\langle S^2 \rangle^{BS}}{\langle S^2 \rangle^{HS} - \langle S^2 \rangle^{BS}} \qquad (5)$$

where E refers to energies, with the superscripts AP, BS, and HS representing the approximately spin-projected state, the broken-symmetry unrestricted singlet state, and high-spin state, respectively. Only triplet was considered in HS because the $\langle S^2 \rangle$ after annihilation was only ~0.03. As a test, the spin-projected ${}^1O_2$ excitation energy was calculated to be 0.89 eV at B3LYP/6-31+G(d,p) and 1.05 eV at BHandHLYP/6-31+G(d,p), which are within ±0.09 eV of the experimental value. It is therefore reasonable to expect that this method would improve the description of reaction PESs. We found that, in addition to ${}^1O_2$, precursor complexes exhibit significant spin contaminations with triplet states; thus, their energies were much improved by the spin-projection method. Open-shell, broken-symmetry calculations of TSs and disulfide peroxides, on the other hand, all converged to closed shells. Natural population charge analysis indicates $[CySS^{+0.85}(OO)^{-0.86} - H]^-$ and $[CySS^{+0.87}(OO)^{-0.80} - 2H]^{2-}$ at TSs, and $[CySS^{+0.85}(OO)^{-0.86} - H]^-$ and $[CySS^{+0.87}(OO)^{-0.97} - 2H]^{2-}$ at peroxides. The zwitterionic characteristics of TSs and end products are consistent with what was found for persulfoxides in reactions of ${}^1O_2$ with sulfides.[13,14,18,61] It may be concluded that spin projection is required mostly at the early stage of the reactions when structures contain loosely bound ${}^1O_2$. We would not expect spin contamination to cause significant issues at the late stage of the reactions when wavefunctions become stable in restricted DFT.

Both spin-projected, open-shell energies (bold lines) and restricted singlet-state energies (dashed lines) are plotted in Figure 5, where reactants are located at zero energy. To verify
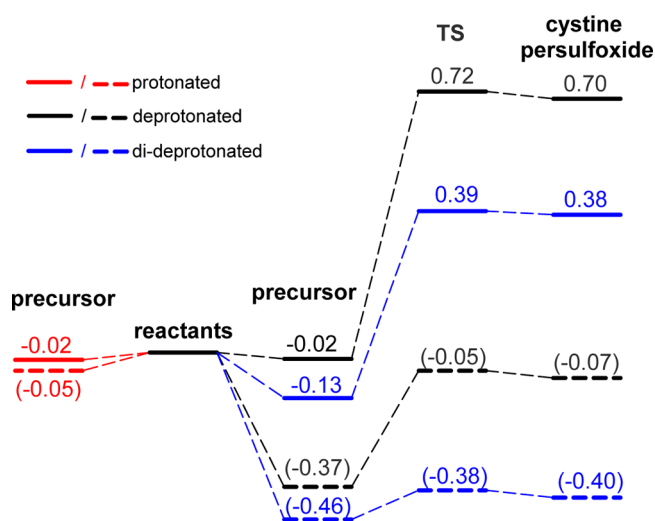

Figure 5. Reaction coordinates for ${}^1O_2$ with $[CySSCy + H]^+$, $[CySSCy - H]^-$, and $[CySSCy - 2H]^{2-}$, calculated at B3LYP/6-31+G(d,p). Solid lines indicate approximately spin-projected, open-shell energies, and dotted lines indicate closed-shell energies. For protonated cystine, only precursor exists.

that the spin-projected results are not functional dependent, we calculated precursors for these systems using BHandHLYP/6-31+G(d,p)—another popular functional set for describing amino acid energies with accuracy better than MP2.[64] The latter was able to reproduce B3LYP results.

The mechanistic importance of the low-lying precursors in Figure 5 depends on their lifetimes, so we used RRKM theory to model their unimolecular kinetics. No barrier was expected for decay of the precursor to reactants in excess of dissociation

asymptote; thus, an orbiting TS[65] was assumed. Rotational quantum number (K) was treated as active in evaluating rate constant $k(E, J)$, and all $(2J + 1)K$ levels were counted as shown by eq 6

$$k(E, J) = \frac{d}{h} \frac{\sum_{K=-J}^{J} G[E - E_0 - E_r^+(J, K)]}{\sum_{K=-J}^{J} N[E - E_r(J, K)]} \qquad (6)$$

where d is the reaction path degeneracy, G is the sum of accessible states from 0 to $E - E_0 - E_r^+$ at the orbiting TS, N is the energized reactant's density of states, E is the system energy, E_0 is the activation energy, and E_r and E_r^+ are the rotational energies of the reactant and the orbiting TS, respectively. Precursors and reactants were described by B3LYP-calculated frequencies, moments of inertia, and spin-projected energies. At the E_{col} regime below 0.2 eV, where a complex-mediated mechanism might be important, the dissociation rate constant is $10^9 - 10^{11}$ s^{-1} for the precursors at different ionization states. This corresponds to a lifetime (<ns) that was insignificant during mass spectrometric measurements (on the time scale of ~10^2 μs). As a result, kinetic analysis predicted no chemical reactivity for cystine ions.

4. CONCLUSIONS

We presented a guided-ion-beam scattering mass spectrometric and theoretical study on the collisions of $^1O_2$ with protonated, deprotonated, and di-deprotonated cystine. Ion−molecule scattering measurements confirmed no oxidation of cystine ions by $^1O_2$ despite the fact that alkyl disulfides are oxidizable. A series of DFT potential surfaces, with the aid of approximately spin-projected open-shell, broken-symmetry calculations, have provided rationalization for experimental results. One remarkable finding is that the collisions of pronated cystine with $^1O_2$ follow a repulsive potential surface starting from the initial approaching of reactants. Formation of short-lived, weak complexes is possible in the collisions of singly and di-deprotonated cystine with $^1O_2$, but their conversions to stable persulfoxides (akin to the key intermediates proposed for oxidation of alkyl sulfides) are hampered by high activation barriers. We reported previously that $^1O_2$ oxidation of Cys[23−25] and Met[26,27] is mediated by hydroperoxide intermediates CySOOH and MetOOH, which are an analogue of (but yet more stable than) the S-hydroperoxysulfonium ylide in $^1O_2$ oxidation of organic sulfides.[6,45,61] The nonreactivitiy of cystine may be traced back to the lack of a mobile proton that would otherwise prompt cystine oxidation via the formation of hydropersulfoxides from peroxide intermediates.

Disulfide bond cleavage (both C−S and S−S cleavages) of disulfide-containing peptides may open access to the previously covered backbone regions and help identify peptide primary structures. Various approaches were reported for inducing disulfide bond cleavage, such as UV photodissociation,[49,66] negative-ion dissociation,[67,68] EID,[52] and radical-induced dissociation.[69,70] The present experiment probed CID of cystine ions, including di-deprotonated cystine for the first time. In contrast to minor disulfide bond cleavage in the CID of protonated cystine, C−S cleavage dominates the CID of di-deprotonated cystine and produces unique $H_2NCH(CO_2^-)$-$CH_2SS^\bullet$ anionic radical fragment.

■ ASSOCIATED CONTENT

S **Supporting Information**

The Supporting Information is available free of charge on the ACS Publications website at DOI: 10.1021/acs.jpcb.7b05674.

Tautomer/rotamers of $[CySSCy + H]^+$, $[CySSCy − H]^-$, and $[CySSCy − 2H]^{2-}$; CID mass spectrum and fragmentation scheme for $[CySSCy + H]^+$; structures in Figures 2d–4 (PDF)

Movies of TS(C−S), $[TS − H]^-$, and $[TS − 2H]^{2-}$ (ZIP)

■ AUTHOR INFORMATION

Corresponding Author

*E-mail: jianbo.liu@qc.cuny.edu. Tel: 1-718-997-3271.

ORCID ⊙

Jianbo Liu: 0000-0001-9577-3740

Notes

The authors declare no competing financial interest.

■ REFERENCES

(1) Ogilby, P. R. Singlet Oxygen: There Is Indeed Something New under the Sun. *Chem. Soc. Rev.* **2010**, *39*, 3181−3209.

(2) Davies, M. J. Reactive Species Formed on Proteins Exposed to Singlet Oxygen. *Photochem. Photobiol. Sci.* **2004**, *3*, 17−25.

(3) Cadet, J.; Ravanat, J.-L.; Martinez, G. R.; Medeiros, M. H. G.; Mascio, P. D. Singlet Oxygen Oxidation of Isolated and Cellular DNA: Product Formation and Mechanistic Insights. *Photochem. Photobiol.* **2006**, *82*, 1219−1225.

(4) Marchetti, B.; Karsili, T. N. V. An Exploration of the Reactivity of Singlet Oxygen with Biomolecular Constituents. *Chem. Commun.* **2016**, *52*, 10996−10999.

(5) Palumbo, G. Photodynamic Therapy and Cancer: A Brief Sightseeing Tour. *Expert Opin. Drug Delivery* **2007**, *4*, 131−148.

(6) Clennan, E. L. Persulfoxide: Key Intermediate in Reactions of Singlet Oxygen with Sulfides. *Acc. Chem. Res.* **2001**, *34*, 875−884.

(7) Thornton, J. M. Disulfide Bridges in Globular Proteins. *J. Mol. Biol.* **1981**, *151*, 261−287.

(8) Hogg, P. J. Disulfide Bonds as Switches for Protein Function. *Trends Biochem. Sci.* **2003**, *28*, 210−214.

(9) Mace, K. A.; Duce, R. A.; Tindale, N. W. Organic Nitrogen in Rain and Aerosol at Cape Grim, Tasmania, Australia. *J. Geophys. Res.* **2003**, *108*, No. D11.

(10) Mader, B. T.; Yu, J. Z.; Xu, J. H.; Li, Q. F.; Hu, W. S.; Flagan, R. C.; Seinfeld, J. H. Molecular Composition of the Water-Soluble Fraction of Atmospheric Carbonaceous Aerosols Collected During ACE-Asia. *J. Geophys. Res.* **2004**, *109*, No. D06206.

(11) Anastasio, C.; McGregor, K. G. Photodestruction of Dissolved Organic Nitrogen Species in Fogwaters. *Aerosol Sci. Technol.* **2000**, *32*, 106−119.

(12) Millington, K. R.; Church, J. S. The Photodegradation of Wool Keratin II. Proposed Mechanisms Involving Cystine. *J. Photochem. Photobiol., B* **1997**, *39*, 204−212.

(13) Foote, C. S.; Peters, J. W. Chemistry of Singlet Oxygen. XIV. Reactive Intermediate in Sulfide Photooxidation. *J. Am. Chem. Soc.* **1971**, *93*, 3795−3796.

(14) Murray, R. W.; Jindal, S. L. Photosensitized Oxidation of Dialkyl Disulfides. *J. Org. Chem.* **1972**, *37*, 3516−3520.

(15) Creed, D. The Photophysics and Photochemistry of the near-UV Absorbing Amino Acids. III. Cystine and Its Simple Derivatives. *Photochem. Photobiol.* **1984**, *39*, 577−583.

(16) Ando, W.; Takata, T. Photooxidation of Sulfur Compounds. In *Singlet O₂*; Frimer, A. A., Ed.; CRC Press: Boca Raton, 1985; Vol. 3: Reaction Modes and Products Part 2, pp 1−117.

(17) Straight, R. C.; Spikes, J. D. Photosensitized Oxidation of Biomolecules. In *Singlet O₂*; Frimer, A. A., Ed.; CRC Press: Boca Raton, Florida, 1985; Vol. 4: Polymers and Biomolecules, pp 91−143.

(18) Murray, R. W.; Jindal, S. L. Photosensitized Oxidation of Disulfides Related to Cystine. *Photochem. Photobiol.* **1972**, *16*, 147−151.

(19) Fliss, H.; Viswanatha, T. 2,3-Butanedione as a Photosensitizing Agent: Application to α-Amino Acids and α-Chymotrypsin. *Can. J. Biochem.* **1979**, *57*, 1267−1272.

(20) Weil, L. On the Mechanism of the Photo-Oxidation of Amino Acids Sensitized by Methylene Blue. *Arch. Biochem. Biophys.* **1965**, *110*, 57−68.

(21) Weil, L.; Gordon, W. G.; Buchert, A. R. Photooxidation of Amino Acids in the Presence of Methylene Blue. *Arch. Biochem. Biophys.* **1951**, *33*, 90−109.

(22) Benassi, C. A.; Scoffone, E.; Galiazzo, G.; Iori, G. Proflavine-Sensitized Photooxidation of Tryptophan and Related Peptides. *Photochem. Photobiol.* **1967**, *6*, 857−866.

(23) Liu, F.; Fang, Y.; Chen, Y.; Liu, J. Dissociative Excitation Energy Transfer in the Reactions of Protonated Cysteine and Tryptophan with Electronically Excited Singlet Molecular Oxygen ($a^1\Delta_g$). *J. Phys. Chem. B* **2011**, *115*, 9898−9909.

(24) Fang, Y.; Liu, F.; Emre, R.; Liu, J. Guided-Ion-Beam Scattering and Direct Dynamics Trajectroy Study on the Reaction of Deprotonated Cysteine with Singlet Molecualar Oxygen. *J. Phys. Chem. B* **2013**, *117*, 2878−2887.

(25) Liu, F.; Emre, R.; Lu, W.; Liu, J. Oxidation of Gas-Phase Hydrated Protonated/Deprotonated Cysteine: How Many Water Ligands Are Sufficient to Approach Solution-Phase Photooxidation Chemistry? *Phys. Chem. Chem. Phys.* **2013**, *15*, 20496−20509.

(26) Fang, Y.; Liu, F.; Bennett, A.; Ara, S.; Liu, J. Experimental and Trajectory Study on Reaction of Protonated Methionine with Electronically Excited Singlet Molecular Oxygen ($a^1\Delta_g$): Reaction Dynamics and Collision Energy Effects. *J. Phys. Chem. B* **2011**, *115*, 2671−2682.

(27) Liu, F.; Liu, J. Oxidation Dynamics of Methionine with Singlet Oxygen: Effects of Methionine Ionization and Microsolvation. *J. Phys. Chem. B* **2015**, *119*, 8001−8012.

(28) Seliger, H. H. A Photoelectric Method for the Measurement of Spectra of Light Sources of Rapidly Varying Intensities. *Anal. Biochem.* **1960**, *1*, 60−65.

(29) Khan, A.; Kasha, M. Red Chemiluminescence of Oxygen in Aqueous Solution. *J. Chem. Phys.* **1963**, *39*, 2105−2106.

(30) Maranzana, A.; Ghigo, G.; Tonachini, G. Diradical and Peroxirane Pathways in the $[\pi2 + \pi2]$ Cycloaddition Reactions of $^1\Delta_g$ Dioxygen with Ethene, Methyl Vinyl Ether, and Butadiene: A Density Functional and Multireference Perturbation Theory Study. *J. Am. Chem. Soc.* **2000**, *122*, 1414−1423.

(31) Szabo, A.; Ostlund, N. S. *Modern Quantum Chemistry: Introduction to Advanced Electronic Structure Theory*; Dover Publications: New York, NY, 1996; p 480.

(32) Saito, T.; Nishihara, S.; Kataoka, Y.; Nakanishi, Y.; Matsui, T.; Kitagawa, Y.; Kawakami, T.; Okumura, M.; Yamaguchi, K. Transition State Optimization Based on Approximate Spin-Projection (AP) Method. *Chem. Phys. Lett.* **2009**, *483*, 168−171.

(33) Saito, T.; Nishihara, S.; Kataoka, Y.; Nakanishi, Y.; Kitagawa, Y.; Kawakami, T.; Yamanaka, S.; Okumura, M.; Yamaguchi, K. Reinvestigation of the Reaction of Ethylene and Singlet Oxygen by the Approximate Spin Projection Method. Comparison with Multireference Coupled-Cluster Calculations. *J. Phys. Chem. A* **2010**, *114*, 7967−7974.

(34) Fang, Y.; Liu, J. Reaction of Protonated Tyrosine with Electronically Excited Singlet Molecular Oxygen ($a^1\Delta_g$): An Experimental and Trajectory Study. *J. Phys. Chem. A* **2009**, *113*, 11250−11261.

(35) Lide, D. R. *CRC Handbook of Chemistry and Physics*; CRC Press: Boca Raton, 2007−2008.

(36) Ervin, K. M.; Armentrout, P. B. Translational Energy Dependence of $Ar^+ + XY \rightarrow ArX^+ + Y$ ($XY = H_2$, D_2, HD) from Thermal to 30 eV C.M. *J. Chem. Phys.* **1985**, *83*, 166−189.

(37) Midey, A.; Dotan, I.; Viggiano, A. A. Temperature Dependences for the Reactions of O^- and O_2^- with $O_2(a^1\Delta_g)$ from 200 to 700 K. *J. Phys. Chem. A* **2008**, *112*, 3040−3045.

(38) Lafferty, W. J.; Solodov, A. M.; Lugez, C. L.; Fraser, G. T. Rotational Line Strengths and Self-Pressure-Broadening Coefficients for the 1.27 Mm, $a^1\Delta_g$-$X^3\sum_g^-$, ν = 0-0 Band of O_2. *Appl. Opt.* **1998**, *37*, 2264−2270.

(39) Frisch, M. J.; Trucks, G. W.; Schlegel, H. B.; Scuseria, G. E.; Robb, M. A.; Cheeseman, J. R.; Scalmani, G.; Barone, V.; Mennucci, B.; Petersson, G. A.; et al. *Gaussian 09*, revision D.01; Gaussian, Inc: Wallingford, CT, 2013.

(40) Alecu, I. M.; Zheng, J.; Zhao, Y.; Truhlar, D. G. Computational Thermochemistry: Scale Factor Databases and Scale Factors for Vibrational Frequencies Obtained from Electronic Model Chemistries. *J. Chem. Theory Comput.* **2010**, *6*, 2872−2887.

(41) Neese, F. The Orca Program System. *Wiley Interdiscip. Rev.: Comput. Mol. Sci.* **2012**, *2*, 73−78.

(42) Glendening, E. D.; Badenhoop, J. K.; Reed, A. E.; Carpenter, J. E.; Bohmann, J. A.; Morales, C. M.; Landis, C. R.; Weinhold, F. *NBO*, version 6.0; Theoretical Chemistry Institute, University of Wiscosin: Madison, WI, 2013.

(43) Marcus, R. A. Unimolecular Dissociations and Free-Radical Recombination Reactions. *J. Chem. Phys.* **1952**, *20*, 359−364.

(44) Zhu, L.; Hase, W. L. *A General RRKM Program (QCPE 644)*, *Quantum Chemistry Program Exchange*; Chemistry Department, University of Indiana: Bloomington, 1993.

(45) McKee, M. L. A Theoretical Study of Unimolecular Reactions of Dimethyl Persulfoxide. *J. Am. Chem. Soc.* **1998**, *120*, 3963−3969.

(46) Lu, W.; Liu, J. Capturing Transient Endoperoxide in the Singlet Oxygen Oxidation of Guanine. *Chem. Eur. J.* **2016**, *22*, 3127−3138.

(47) Lu, W.; Teng, H.; Liu, J. How Protonation and Deprotonation of 9-Methylguanine Alter Its Singlet O_2 Addition Path: About the Initial Stage of Guanine Nucleoside Oxidation. *Phys. Chem. Chem. Phys.* **2016**, *18*, 15223−15234.

(48) Thapa, B.; Munk, B. H.; Burrows, C. J.; Schlegel, H. B. Computational Study of Oxidation of Guanine by Singlet Oxygen ($^1\Delta_g$) and Formation of Guanine:Lysine Cross-Links. *Chem. Eur. J.* **2017**, *23*, 5804−5813.

(49) Soorkia, S.; Dehon, C.; Kumar, S. S.; Pedrazzani, M.; Frantzen, E.; Lucas, B.; Barat, M.; Fayeton, J. A.; Jouvet, C. UV Photo-fragmentation Dynamics of Protonated Cystine: Disulfide Bond Rupture. *J. Phys. Chem. Lett.* **2014**, *5*, 1110−1116.

(50) Burrows, E. P. Dimethyl Ether Chemical Ionization Mass Spectrometry of α-Amino Acids. *J. Mass Spectrom.* **1998**, *33*, 221−228.

(51) Lioe, H.; O'Hair, R. A. J. A Novel Salt Bridge Mechanism Highlights the Need for Nonmobile Proton Conditions to Promote Disulfide Bond Cleavage in Protonated Peptides under Low-Energy Collisional Activation. *J. Am. Soc. Mass Spectrom.* **2007**, *18*, 1109−1123.

(52) Lioe, H.; O'Hair, R. A. J. Comparison of Collision-Induced Dissociation and Electron-Induced Dissociation of Singly Protonated Aromatic Amino Acids, Cystine and Related Simple Peptides Using a Hybrid Linear Ion Trap−FT-ICR Mass Spectrometer. *Anal. Bioanal. Chem.* **2007**, *389*, 1429−1437.

(53) Rubino, F. M.; Verduci, C.; Giampiccolo, R.; Pulvirenti, S.; Brambilla, G.; Colombi, A. Characterization of the Disulfides of Bio-Thiols by Electrospray Ionization and Triple-Quadrupole Tandem Mass Spectrometry. *J. Mass Spectrom.* **2004**, *39*, 1408−1416.

(54) Ghumman, C. A. A.; Moutinho, A. M. C.; Santos, A.; Tolstogouzov, A.; Teodoro, O. M. N. D. TOF-SIMS Study of Cystine and Cholesterol Stones. *J. Mass Spectrom.* **2012**, *47*, 547−551.

(55) Wang, L.-S.; Ding, C.-F.; Wang, X.-B.; Nicholas, J. B. Probing the Potential Barriers and Intramolecular Electrostatic Interactions in Free Doubly Charged Anions. *Phys. Rev. Lett.* **1998**, *81*, 2667−2670.

(56) Dreuw, A.; Cederbaum, L. S. Multiply Charged Anions in the Gas Phase. *Chem. Rev.* **2002**, *102*, 181−200.

(57) Smith, R. D.; Loo, J. A.; Barinaga, C. J.; Edmonds, C. G.; Udseth, H. R. Collisional Activation and Collision-Activated Dissociation of Large Multiply Charged Polypeptides and Proteins Produced by Electrospray Ionization. *J. Am. Soc. Mass Spectrom.* **1990**, *1*, 53−65.

(58) McLuckey, S. A.; Glish, G. L.; Berkel, G. J. V. Charge Determination of Product Ions Formed from Collision- Induced Dissociation of Multiply Protonated Molecules Via Ion/Molecule Reactions. *Anal. Chem.* **1991**, *63*, 1971−1978.

(59) Liu, J.; van Devener, B.; Anderson, S. L. Vibrational Mode and Collision Energy Effects on Reaction of H_2CO^+ with C_2D_4. *J. Chem. Phys.* **2004**, *121*, 11746−11759.

(60) Troe, J. Statistical Adiabatic Channel Model of Ion-Neutral Dipole Capture Rate Constants. *Chem. Phys. Lett.* **1985**, *122*, 425−430.

(61) Jensen, F.; Greer, A.; Clennan, E. L. Reaction of Organic Sulfides with Singlet Oxygen. A Revised Mechanism. *J. Am. Chem. Soc.* **1998**, *120*, 4439−4449.

(62) Lu, W.; Liu, J. Deprotonated Guanine·Cytosine and 9-Methylguanine·Cytosine Base Pairs and Their "Non-Statistical" Kinetics: A Combined Guided-Ion Beam and Computational Study. *Phys. Chem. Chem. Phys.* **2016**, *18*, 32222−32237.

(63) Levine, R. D.; Bernstein, R. B. *Molecular Reaction Dynamics and Chemical Reactivity*; Oxford University Press: New York, 1987.

(64) Yu, W.; Liang, L.; Lin, Z.; Ling, S.; Haranczyk, M.; Gutowski, M. Comparison of Some Representative Density Functional Theory and Wave Function Theory Methods for the Studies of Amino Acids. *J. Comput. Chem.* **2009**, *30*, 589−600.

(65) Rodgers, M. T.; Ervin, K. M.; Armentrout, P. B. Statistical Modeling of Collision-Induced Dissociation Thresholds. *J. Chem. Phys.* **1997**, *106*, 4499−4508.

(66) Fung, Y. M. E.; Kjeldsen, F.; Silivra, O. A.; Chan, T. W. D.; Zubarev, R. A. Facile Disulfide Bond Cleavage in Gaseous Peptide and Protein Cations by Ultraviolet Photodissociation at 157 nm. *Angew. Chem., Int. Ed.* **2005**, *44*, 6399−6403.

(67) Chrisman, P. A.; McLuckey, S. A. Dissociations of Disulfide-Linked Gaseous Polypeptide/Protein Anions: Ion Chemistry with Implications for Protein Identification and Characterization. *J. Proteome Res.* **2002**, *1*, 549−557.

(68) Zhang, M.; Kaltashov, I. A. Mapping of Protein Disulfide Bonds Using Negative Ion Fragmentation with a Broadband Precursor Selection. *Anal. Chem.* **2006**, *78*, 4820−4829.

(69) Xia, Y.; Cooks, R. G. Plasma Induced Oxidative Cleavage of Disulfide Bonds in Polypeptides During Nanoelectrospray Ionization. *Anal. Chem.* **2010**, *82*, 2856−2864.

(70) Stinson, C. A.; Xia, Y. Radical Induced Disulfide Bond Cleavage within Peptides Via Ultraviolet Irradiation of an Electrospray Plume. *Analyst* **2013**, *138*, 2840−2846.